

The Deuterium Fractionation Timescale in Dense Cloud Cores: A Parameter Space Exploration

Shuo Kong^{1*}, Paola Caselli², Jonathan C. Tan^{1,3} and Valentine Wakelam^{4,5}

¹*Dept. of Astronomy, University of Florida, Gainesville, Florida 32611, USA*

²*School of Physics and Astronomy, University of Leeds, Leeds LS2 9JT, UK*

³*Dept. of Physics, University of Florida, Gainesville, Florida 32611, USA*

⁴*University of Bordeaux, LAB, UMR 5804, 33270, Floirac, France*

⁵*CNRS, LAB, UMR 5804, 33270, Floirac, France*

Accepted. Received; in original form

ABSTRACT

The deuterium fraction of simple species such as N_2H^+ can be easily measured and can provide information about the age of dense and cold material, important to compare with dynamical models of cloud core formation and evolution. Here we perform a parameter space exploration using a gas-phase chemical model which includes deuterium chemistry and the spin states of H_2 and H_3^+ isotopologues. This allows us to study the effect of various poorly known parameters on the timescale to achieve the deuterium fractions observed in starless cores and clumps in various star-forming regions. We conclude that for a broad range of parameters, the relatively large deuterium fractions ($\gtrsim 0.1$) observed towards both low- and high-mass starless cores require core ages to be at least a few times longer than the free-fall timescale. This condition could be relaxed if cosmic ray ionization rates are very high $\gtrsim 10^{-16} \text{ s}^{-1}$ or initial ortho-to-para ratios of H_2 are very low ($\lesssim 10^{-2}$), although the latter itself requires the parental molecular cloud to be relatively old. These results suggest that a mechanism exists, most likely magnetic field support, to prevent the dense cores from collapsing rapidly, consistent with the observed line profiles of high-density tracers.

Key words: Physical data and processes: astrochemistry – stars: formation – ISM: clouds.

1 INTRODUCTION

Deuterated molecules are useful tools to study the cold and dense environments where stars are born. This has been demonstrated in low-mass star-forming regions (e.g., Caselli 2002; Bacmann et al. 2003; Crapsi et al. 2005, 2007; Emprechtinger et al. 2009; Friesen et al. 2010) as well as in regions thought to be precursors of massive stars and stellar clusters (e.g., Fontani et al. 2006, 2009, 2011; Pillai et al. 2007, 2012). Deuterated species can be used to infer the elusive electron fraction $x(e)$ (e.g., Guelin et al. 1977; Wootten et al. 1979; Caselli et al. 1998; Bergin et al. 1999; Dalgarno 2006, although the equations in these papers need to be modified to include the doubly and triply deuterated forms of H_3^+) and the age of molecular clouds (Pagani, Roueff & Lesaffre 2011; Pagani et al. 2013). Electron fraction and cloud age are two important parameters to shed light on the dynamical evolution of star-forming re-

gions, as the ambipolar diffusion timescale is directly proportional to $x(e)$ (e.g., Shu, Adams & Lizano 1987) and the age can put stringent constraints on the mechanism(s) regulating cloud core formation (e.g., magnetic field, turbulence and shocks). However, variations in the cosmic-ray ionization rate, the volume density, the kinetic temperature, rates of molecular freeze-out onto dust grain surfaces and the ortho-to-para ratio of H_2 make attempts to fix these values rather uncertain, especially for regions with poorly known physical structure. Recently, Pagani et al. (2013) investigated these effects by coupling dynamics with chemistry. They developed a chemical clock to derive the age of low-mass cores and extensively discussed the role of ortho- H_2 . In this paper, we focus on the age of cloud cores as determined by the measured deuterium fraction in simple species such as N_2H^+ , which is similar to Pagani et al. (2013) but extended to include conditions relevant to high-mass cores, and explore uniformly the parameter space without any prior assumption about the rather uncertain dynamical history, to

* E-mail: skong@astro.ufl.edu

assess the importance of the above mentioned quantities in the determination of cloud age.

The astrochemical model is described in §2, results are shown in §3 and discussed in §4. The conclusions are listed in §5.

2 METHODS

We utilize the numerical code Nahoon (Wakelam et al. 2012), and the reaction network is a reduced network downloaded from the online KIDA¹ database (Wakelam et al. 2012) (October 2010 version, updated later, see below). The reduced network includes the elements H, He, O, C and N, and all molecules and molecular ions up to three atoms in size. The validity of the reduction has been tested against a more complete network. We augmented the reduced network by addition of deuterium atoms, deuterated species and the spin states of H₂, H₃⁺ and its deuterated isotopologues, following prescriptions of Walmsley, Flower & Pineau des Forêts (2004); Flower, Pineau Des Forêts & Walmsley (2006); Hugo, Asvany & Schlemme (2009); Pagani et al. (2009); Sipilä et al. (2010) and selecting the most recent values for the rate coefficients. Dissociative recombination rates for all the forms of H₃⁺ have been calculated using an interpolation routine which reads Table B.1 of Pagani et al. (2009). Surface chemistry is not included, except for the formation of para-H₂, ortho-H₂, HD, para-D₂ and ortho-D₂. The rates have been calculated following Pagani et al. (2009), where the formation rate coefficient (in cm³ s⁻¹) of HD is 0.5 times that of H₂ and of D₂ is 10⁻⁵ times that of H₂. The ortho-to-para ratio upon surface formation has been assumed equal to the statistical value of 3 for H₂ and 2 for D₂. Neutral and negatively charged grains are considered. Coulomb focusing was taken into account for reactions involving positively charged ions on negatively charged grains (Draine & Sutin 1987). The final chemical network includes 2987 reactions involving 128 different species. More details can be found in §3.3 of Vastel et al. (2012), where the code has been used to interpret ground-based and Herschel Space Observatory observations of deuterated isotopologues of H₃⁺ toward a pre-stellar core. Compared to the model used in Vastel et al. (2012), the present version of the code has been updated through detailed benchmarking with the gas phase network of Sipilä, Caselli & Harju (2013) and, as already mentioned, dissociative recombination for all H₃⁺ forms is now done following Pagani et al. (2009) prescriptions. Small differences are present between our code and that of Sipilä, Caselli & Harju (2013), which is based on osu_03_2008² from the OSU code, while our code includes the 2011 updates from KIDA.

2.1 The Fiducial Model

Before the parameter-space exploration, we present the fiducial model, where the gas number density (expressed via

Table 1. Parameters of the fiducial model.

Parameter	Description	Fiducial model value
n_{H}	number density of H	$1.0 \times 10^5 \text{ cm}^{-3}$
T	temperature	15 K
ζ	cosmic-ray ionization rate	$2.5 \times 10^{-17} \text{ s}^{-1}$
f_{D}	depletion factor	10
G_0	ratio to Habing field	1
A_{V}	visual extinction	30 mag
α	dust-to-gas mass ratio	0.01
a_0	dust particle radius	$1.0 \times 10^{-5} \text{ cm}$
ρ_{GRAIN}	dust grain mass density	3.0 g cm^{-3}

Table 2. Initial elemental abundances in the fiducial model.

Species	Abundance $n_{\text{spec}}/n_{\text{H}}$
pH ₂	1.25×10^{-01}
oH ₂	3.75×10^{-01}
HD	1.50×10^{-05}
He	1.40×10^{-01}
N	2.10×10^{-06}
O	1.80×10^{-05}
C ⁺	7.30×10^{-06}
GRAIN0	1.32×10^{-12}

the number density of H nuclei, n_{H}), temperature and elemental freeze-out are chosen based on typical values measured toward low- and high-mass pre-stellar cores (e.g. Ward-Thompson, Motte & Andre 1999; Crapsi et al. 2005, 2007; Pillai et al. 2006; Hernandez et al. 2011; Ragan et al. 2011; Butler & Tan 2012). Table 1 lists the values of all the parameters in the fiducial model. The value of the cosmic-ray ionization rate is adopted from van der Tak & van Dishoeck (2000). The dust-to-gas mass ratio, grain radius and density are taken from the original Nahoon model and they represent the fiducial values typically adopted in chemical models. The fiducial visual extinction, A_{V} , is set to 30 mag, a value large enough so that photochemistry is unimportant for our adopted radiation field (standard Habing field, $G_0 = 1$). We will consider models with A_{V} as low as 10 mag, but even here photochemistry is insignificant. We assume that refractory metals of low ionization potential (such as Mg and Fe) and polycyclic aromatic hydrocarbons (PAHs), important for the ionization structure, are not present in the gas phase (see Caselli et al. 1998; Wakelam & Herbst 2008, for the effects of metals and PAHs, respectively, on the chemical structure of molecular clouds).

The initial fractional abundances of elements, with respect to total H nuclei are listed in Table 2. All species are assumed to be in atomic form, except for hydrogen. The ortho-to-para H₂ ratio is initially set to its statistical value of 3, obtained in the process of H₂ formation on dust grain surfaces. Deuterium is also assumed to be all in HD form, with a fractional abundance adopted from the measurement of the elemental [D]/[H] ratio measured in our Galaxy ([D]/[H] $\sim 1.5 \times 10^{-5}$; e.g. Oliveira et al. 2003).

¹ <http://kida.obs.u-bordeaux1.fr/>

² See <http://www.physics.ohio-state.edu/~eric/>

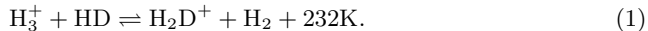
2.2 Comparison to previous methods

In general, we have a richer and more complete chemical network compared to Pagani et al. (2013), who consider 35 species and about 400 reactions in total. Our reaction list includes the latest rate coefficients until July 2013. The effect of this consideration will be discussed later in the results section. Pagani et al. (2013) included heating/cooling and time-dependent CO depletion, however, our current goal is to perform a more systematic study focussing on the chemistry, so that we can have a better understanding of the effects of the initial physical conditions on the chemical composition, ignoring for now the extra complication of the dynamics, which will be considered in a later stage. Pagani et al. (2013) also noticed possible influence of initial ortho-to-para ratio of H_2 and cosmic-ray ionization rate. We will compare our results with theirs later in the results section.

3 RESULTS

3.1 The Fiducial Model

Fig. 1 shows the fractional abundances ($n_{\text{species}}/n_{\text{H}}$) of important species as a function of time in the fiducial model. Four types of species are included in the figure: hydrogen ions, H_2 , H_3^+ and their deuterated isotopologues (plus spin states), and electrons, C-bearing species, O-bearing species, and N-bearing species. As the gas evolves under these cold, dense conditions, the deuteration becomes active through the exothermic reaction (only true in the respective para states of reactants and products; Pagani, Salez, & Wannier 1992):



The abundance of deuterated H_3^+ (H_2D^+ , D_2H^+ , and D_3^+) increases, along with other deuterated species. For instance, H_2D^+ can cede a deuteron to major neutral species, such as CO and N_2 , producing DCO^+ and N_2D^+ , respectively. As a consequence, the deuterium fraction (i.e., defined by the abundance ratios $[\text{N}_2\text{D}^+]/[\text{N}_2\text{H}^+]$, $[\text{DCO}^+]/[\text{HCO}^+]$) starts to overcome the cosmic abundance of deuterium. Hereafter, we denote the deuterium fraction of a certain species as $D_{\text{frac}}^{\text{species}}$ (e.g. $[\text{N}_2\text{D}^+]/[\text{N}_2\text{H}^+] \equiv D_{\text{frac}}^{\text{N}_2\text{H}^+}$) and the spin-state ratio as $\text{OPR}^{\text{species}}$ (e.g., $[\text{ortho-H}_2]/[\text{para-H}_2] \equiv \text{OPR}^{\text{H}_2}$). We will focus on $D_{\text{frac}}^{\text{N}_2\text{H}^+}$ in our study, since HCO^+ suffers more from depletion than N_2H^+ (especially in the central core), so that $D_{\text{frac}}^{\text{N}_2\text{H}^+}$ is a better tool for tracing the inner and denser region of starless/pre-stellar cores (Caselli et al. 2002; Crapsi et al. 2005).

The deuterium fraction significantly increases only at times later than 10^5 yr, when the abundance of ortho- H_2 starts to drop (Fig. 2). In fact, deuteration can be suppressed by ortho- H_2 , which can drive reaction (1) backwards, as originally pointed out by Pineau des Forets, Flower, & McCarroll (1991) (for para- H_2D^+) and Pagani, Salez, & Wannier (1992) (for ortho- H_2D^+), and later discussed by Flower, Pineau Des Forêts & Walmsley (2006); Pagani et al. (2009); Pagani, Roueff & Lesaffre (2011). The conversion of ortho- H_2 to para- H_2 mainly proceeds

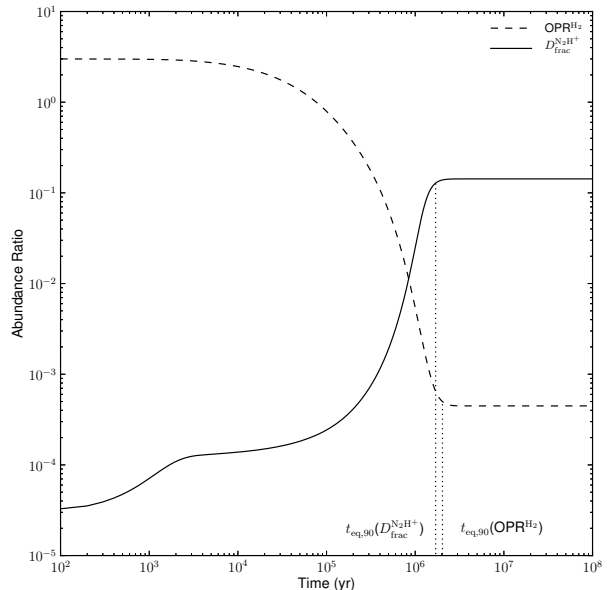


Figure 2. Time-dependence of OPR^{H_2} and $D_{\text{frac}}^{\text{N}_2\text{H}^+}$ in the fiducial model. See §3.1 for the description of the fiducial model and the notation definition.

through the reactions of ortho- H_2 with H^+ and H_3^+ . Fig. 2 shows the time-dependent change of OPR^{H_2} and $D_{\text{frac}}^{\text{N}_2\text{H}^+}$ in the fiducial model: as expected, $D_{\text{frac}}^{\text{N}_2\text{H}^+}$ goes up as OPR^{H_2} drops. After reaching the equilibrium steady-state at $\gtrsim 1$ million years, $D_{\text{frac}}^{\text{N}_2\text{H}^+}$ has increased by ~ 4 orders of magnitude relative to the cosmic deuterium to hydrogen abundance ratio, while OPR^{H_2} drops by more than 3 orders of magnitude. One can also see from Fig. 1 that all species reach steady-state when OPR^{H_2} does. All these point out that OPR^{H_2} is crucial for cold gas chemistry in general, for deuterium fractionation in particular and for the chemical timescale (see §3.3.2).

One thing to note is that in our model, molecules of heavy elements such as CO and N_2 increase with time (Fig. 1). As CO and N_2 are both important destruction partners of H_3^+ and its deuterated isotopologues, they tend to reduce the deuterium fractionation at late stages, though this effect is dominated by ortho- H_2 . Moreover, at the physical conditions of the fiducial model, they should significantly freeze-out onto the dust grains (e.g. Caselli et al. 1999). Since our model currently does not include surface chemistry (except for the formation of H_2 , HD and D_2 and electronic recombination of positively charged ions), the freeze-out process is not included (its effects will be considered in a future paper). Molecular freeze-out is mimicked here by reducing the initial elemental abundances of species heavier than He by the so-called depletion factor f_{D} ($= 10$ for the fiducial model, fixed in each run). Thus, we do not include any differential freeze-out mechanism for CO and N_2 , as laboratory work has found similar sticking coefficients and binding energies for the two molecules (Bisschop et al. 2006). Nevertheless, we note from Fig. 1, that the $\text{N}_2\text{H}^+/\text{CO}$ ratio increases with time, up to a few times 10^5 yr, when the N_2H^+ abundance reaches steady state, as N_2 , the precursor molecule to N_2H^+ , forms more slowly than CO, via neutral-

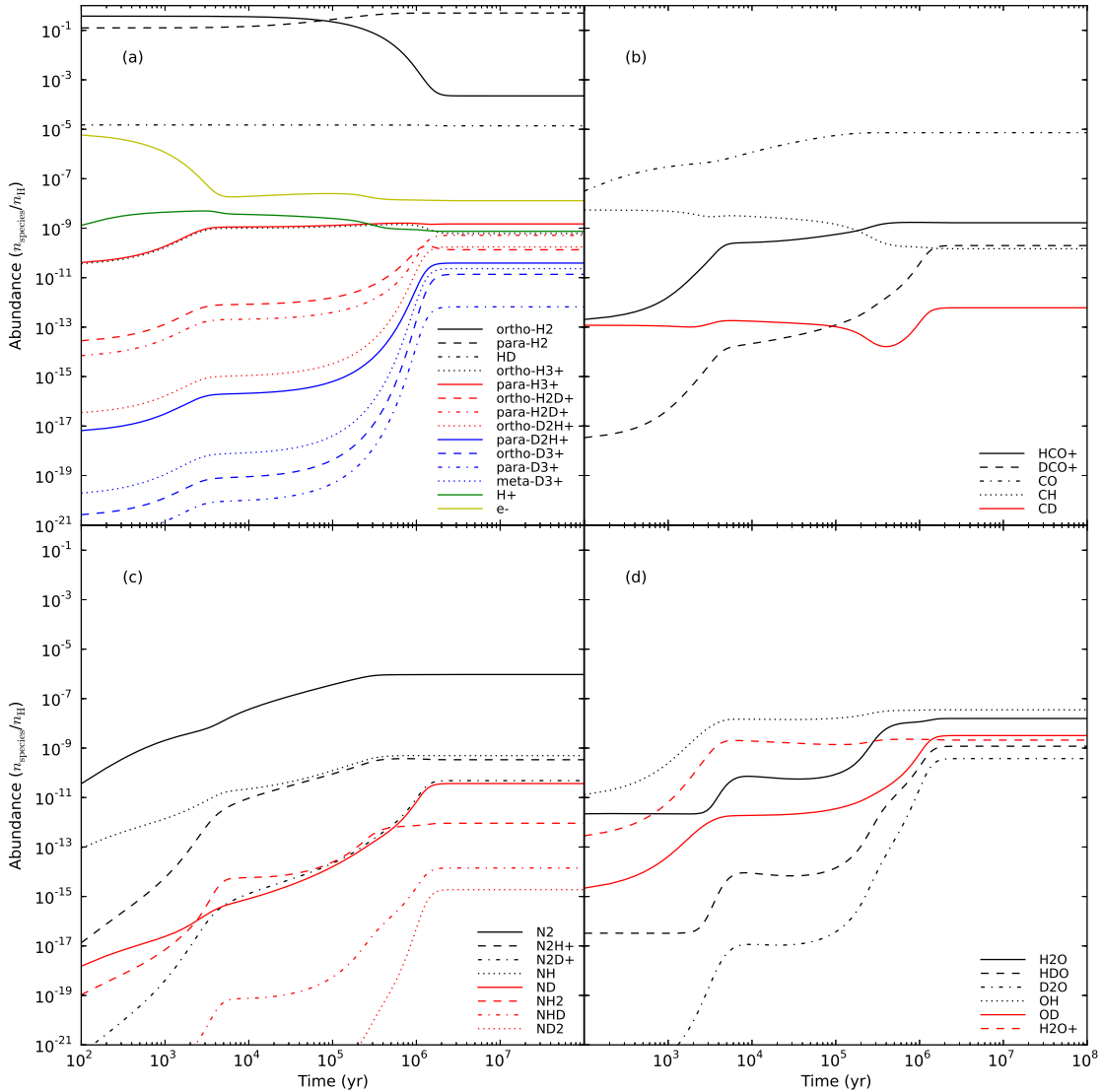


Figure 1. Fractional abundances of important species in the fiducial model. **(a):** hydrogen ions, H_2 , H_3^+ and their deuterated isotopologues (plus spin states), and electrons. **(b):** C-bearing species. **(c):** N-bearing species. **(d):** O-bearing species.

neutral reactions rather than ion-neutral reactions (see also Hily-Blant et al. 2010).

3.2 The deuteration timescale

Studies have suggested a theoretical relation between the deuterium fraction and the evolutionary stage in low-mass cores (Caselli 2002; Crapsi et al. 2005; Pagani et al. 2013), with the level of deuteration rising with the age and increasing density of the starless core, before then falling once a protostar forms and starts to heat its natal envelope. Fontani et al. (2011) have examined a similar relation in massive cores, and their findings support the use of deuterium fraction as an age and/or evolutionary indicator for massive starless and star-forming cores. Here we investigate the timescale for the growth of the deuterium fraction and its implication for the ages of low-mass and massive starless cores. We also examine how the variation of physical prop-

erties of the gas influences this deuteration timescale, i.e. a chemical timescale, and compare to physical timescales, such as the free-fall time t_{ff} and ambipolar diffusion time t_{ad} .

For convenience, when considering the output of our chemical network, we define the equilibrium deuterium fraction, $D_{\text{frac,eq}}$ as the average of two adjacent outputs of D_{frac} (separated by $\Delta t = 10^4$ yr) that have a fractional change of less than $\epsilon = 5 \times 10^{-5}$, i.e.

$$|\Delta D_{\text{frac}}|/D_{\text{frac}} < \epsilon. \quad (2)$$

In practice, we run the model for 10^8 yr and then search backwards in time for when this condition is satisfied. We denote the timescale to reach the equilibrium condition defined by Eq. (2) as $t_{\text{eq}}(D_{\text{frac}}^{\text{species}})$. The equilibrium value of the ortho-to-para ratio of H_2 , $\text{OPR}_{\text{eq}}^{\text{H}_2}$, is defined in a similar way, and the timescale is denoted $t_{\text{eq}}(\text{OPR}^{\text{H}_2})$. In practice, since the evolution of $D_{\text{frac}}^{\text{N}_2\text{H}^+}$ and $\text{OPR}_{\text{eq}}^{\text{H}_2}$ are very slow as

they approaches equilibrium (e.g. Fig. 2), we also define a more representative equilibrium timescale $t_{\text{eq},90}(D_{\text{frac}}^{\text{N}_2\text{H}^+})$ as the time when $D_{\text{frac}}^{\text{N}_2\text{H}^+}$ increases to 90% of $D_{\text{frac,eq}}^{\text{N}_2\text{H}^+}$. In a similar way, we define $t_{\text{eq},90}(\text{OPR}^{\text{H}_2})$ as the time when OPR^{H_2} decreases to $\text{OPR}_{\text{eq}}^{\text{H}_2}/0.90$.

The free-fall timescale is

$$t_{\text{ff}} = \left(\frac{3\pi}{32G\rho} \right)^{1/2} = 1.39 \times 10^5 \left(\frac{10^5 \text{ cm}^{-3}}{n_{\text{H}}} \right)^{1/2} \text{ yr.} \quad (3)$$

As one can see from the first line of Table 3, for the fiducial model with $n_{\text{H}} = 10^5 \text{ cm}^{-3}$, the deuteration timescale $t_{\text{eq},90}(D_{\text{frac}}^{\text{N}_2\text{H}^+})$ is $\sim 10 t_{\text{ff}}$. Thus, if a starless core were to be observed with physical and environmental properties equal to the fiducial model, and $D_{\text{frac}} \gtrsim 0.1$, then our modeling implies it would need to be substantially older than its t_{ff} , assuming it had started with our adopted initial conditions, including the initial OPR of H_2 . We will now examine the dependence of this result on these initial conditions.

3.3 Effect of initial conditions on the deuteration timescale

Before our exploration of parameter space of the physical and environmental core properties, described in §3.4, we focus here on the choice of the initial elemental abundances, including ortho and para H_2 , to explore their effect on the deuteration timescale, and in particular on it being relatively long compared to t_{ff} .

3.3.1 Initial elemental abundances

As shown in Table 2, the fiducial model starts with H in molecular form, D in HD, while He, N, O are in atomic form and C is in ionised form, as expected in the low visual extinction regions surrounding dense cores and within which dense cores form. However, the initial fraction of D in HD is not constrained. Moreover, when dense cores form in molecular clouds, a large fraction of CO and N_2 should already be present (see also Li et al. 2013). There is some evidence that a significant fraction of the nitrogen is still in atomic form in dense cores due to the slow conversion from N to N_2 , but the exact amount is unclear (Hily-Blant et al. 2010). As different initial abundances could affect the $D_{\text{frac}}^{\text{species}}$ and $t_{\text{eq},90}(D_{\text{frac}}^{\text{species}})$, we quantify these effects considering 3 variations to the fiducial model described in §2.1: (1) “atomic D”, where D is in atomic form, compared to the fiducial model, assuming that H_2 is in molecular form in the range of densities and physical conditions assumed here; (2) “fully molecular”, where everything starts in molecular form (all N in N_2 , all C^+ in CO, with the leftover Oxygen left in atomic form); (3) “half N in N_2 ”, where half of the Nitrogen is left in atomic form compared to “fully molecular” case.

Fig. 3 shows the results of these tests, focussing on the changing of $D_{\text{frac}}^{\text{N}_2\text{H}^+}$ and OPR^{H_2} . Table 3 lists the equilibrium ratios and timescales. The equilibrium ratios are not affected by the choice on initial atomic versus molecular abundances. In addition, the different initial setups have little effect ($\lesssim 1\%$) on the timescales.

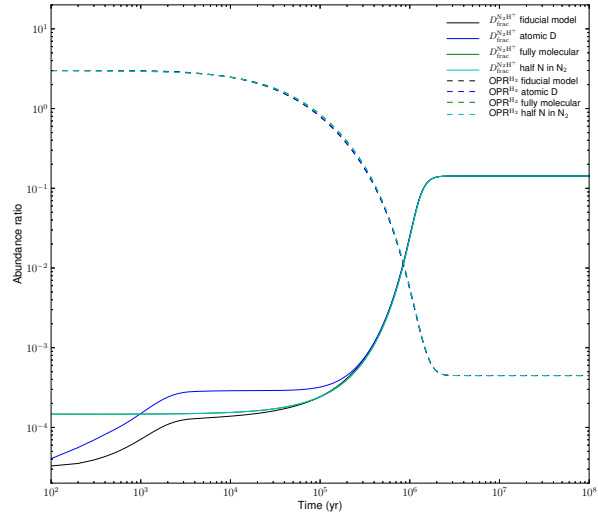


Figure 3. The time-dependent change of OPR^{H_2} and $D_{\text{frac}}^{\text{N}_2\text{H}^+}$ with 4 sets of initial elemental abundances. See §3.3.1 for the description of these sets. The equilibrium ratios and times are summarized in Table 3.

3.3.2 Initial OPR^{H_2}

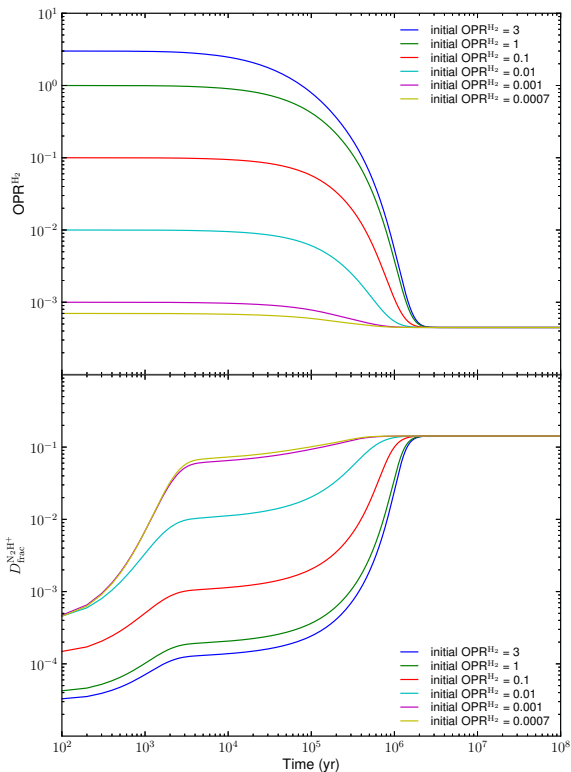
Another poorly constrained, but crucial, parameter is the initial OPR^{H_2} . Only a few observational works have tried to put constraints on this parameter: in diffuse clouds, Crabtree et al. (2011) measured $\text{OPR}^{\text{H}_2} \simeq 0.3\text{--}0.8$; in the pre-stellar core L183, Pagani et al. (2009) derived $\text{OPR}^{\text{H}_2} \simeq 0.1$ (see also Pagani, Roueff & Lesaffre 2011), while Troscompt et al. (2009) estimated $\text{OPR}^{\text{H}_2} \simeq 0$ toward the starless Bok globule B68 (see also discussion in Flower, Pineau Des Forêts & Walmsley 2006; Sipilä, Caselli & Harju 2013). Evidently, different environmental conditions strongly affect OPR^{H_2} (as also deduced by Caselli et al. 2008, in their study of ortho- H_2D^+ in star forming regions).

The fiducial model starts with $\text{OPR}^{\text{H}_2} = 3$, which implies that all H_2 molecules are initially in their statistical spin ratio, as expected if they are just being formed on the surface of dust grains, i.e. if the molecular cloud is very young. However, this may not be the case, based on the above mentioned observations in diffuse clouds and if cloud cores form at a later stage compared to the formation of the parent molecular cloud. To explore this, we consider the effect of different initial OPR^{H_2} values in the fiducial model. Fig. 4 shows their effects on the time evolution of OPR^{H_2} and $D_{\text{frac}}^{\text{N}_2\text{H}^+}$. The different initial OPR^{H_2} values have little effect on both $\text{OPR}_{\text{eq}}^{\text{H}_2}$ and $D_{\text{frac,eq}}^{\text{N}_2\text{H}^+}$, but the timescales to reach equilibrium are affected (as also found by Pagani, Roueff & Lesaffre 2011, see their Fig. 2). Since the $\text{OPR}_{\text{eq}}^{\text{H}_2}$ is 4.48×10^{-4} , the lower the initial OPR^{H_2} , the sooner chemical equilibrium will be reached. We find $t_{\text{eq},90}(D_{\text{frac}}^{\text{N}_2\text{H}^+})$ becomes comparable to t_{ff} if OPR^{H_2} is initially 0.001 or lower. This is also summarized in Table 4. These results suggest that we should consider how evolved the parent cloud is before being confident in the estimate of a core’s chemical age.

In Appendix A, we investigate the evolution of OPR^{H_2}

Table 3. The equilibrium ratios and timescales for the models shown in Fig. 3.

Models	$\text{OPR}_{\text{eq}}^{\text{H}_2}$ ($\times 10^{-4}$)	$t_{\text{eq}}(\text{OPR}^{\text{H}_2})$ (10^6 yr)	$t_{\text{eq},90}(\text{OPR}^{\text{H}_2})$ (10^6 yr)	$D_{\text{frac,eq}}^{\text{N}_2\text{H}^+}$	$t_{\text{eq}}(D_{\text{frac}}^{\text{N}_2\text{H}^+})$ (10^6 yr)	$t_{\text{eq},90}(D_{\text{frac}}^{\text{N}_2\text{H}^+})$ (10^6 yr)
fiducial	4.48	3.14	2.03	0.142	2.78	1.70
atomic D	4.48	3.14	2.03	0.142	2.78	1.70
fully molecular	4.48	3.14	2.04	0.142	2.78	1.71
half N in N_2	4.48	3.14	2.04	0.142	2.78	1.71

**Figure 4.** The evolution of OPR^{H_2} and $D_{\text{frac}}^{\text{N}_2\text{H}^+}$ under different assumptions of initial OPR^{H_2} . We explore initial OPR^{H_2} from 3 (the fiducial model) down to 7×10^{-4} . Note that $\text{OPR}_{\text{eq}}^{\text{H}_2} \simeq 4.5 \times 10^{-4}$.

in the parental cloud. If the cloud has been molecular for $\lesssim 2$ Myr, then OPR^{H_2} is typically expected to be $\gtrsim 0.01$, unless the cosmic ray ionisation rate is significantly larger than the fiducial value. However, parental clouds older than a few Myr do have the chance to reach low, ~ 0.001 , values of OPR^{H_2} . Thus estimates of core deuteration timescales presented in the following sections are contingent on the assumption that the core does not start forming with such low values of OPR^{H_2} .

3.4 Effect of physical and environmental properties on starless cores

Here we present a parameter space exploration to see how different physical conditions affect the chemical evolution of gas in starless cores, assuming an initial $\text{OPR}^{\text{H}_2} = 3$ (Appendix A presents results for $\text{OPR}^{\text{H}_2} = 1, 0.1, 0.01$). In particular, we vary four parameters: the H number density n_{H}

from 10^3 to 10^7 cm^{-3} , the temperature T from 5 to 30 K, the cosmic-ray ionization rate ζ from 10^{-18} to 10^{-15} s^{-1} , the gas phase depletion factor f_D from 1 to 1000 ($f_D = 1$ implies no depletion).

Fig. 5 shows the effect on the evolution of OPR^{H_2} and $D_{\text{frac}}^{\text{N}_2\text{H}^+}$ of varying these four parameters. In general, n_{H} and T have a greater influence on $D_{\text{frac,eq}}^{\text{N}_2\text{H}^+}$, while ζ and f_D affect both $D_{\text{frac,eq}}^{\text{N}_2\text{H}^+}$ and OPR^{H_2} . This implies that the physical environment plays an important role in dense core chemistry. It is thus crucial to choose appropriate conditions for the model before comparing with observations.

Fig. 6 shows the equilibrium ratios and timescales of OPR^{H_2} (upper 2 rows) and $D_{\text{frac}}^{\text{N}_2\text{H}^+}$ (lower 2 rows). One thing to note is that the equilibrium time profile of $D_{\text{frac}}^{\text{N}_2\text{H}^+}$ (fourth row) is almost identical to that of OPR^{H_2} (second row). The two ratios are tightly related. In the following, we summarize their dependence on each physical quantity, with emphasis on $D_{\text{frac}}^{\text{N}_2\text{H}^+}$ (observationally obtainable) and $t_{\text{eq},90}(D_{\text{frac}}^{\text{N}_2\text{H}^+})$.

3.4.1 Dependence on n_{H}

As shown in panel (i) of Fig. 6, a denser core will have a higher $D_{\text{frac,eq}}^{\text{N}_2\text{H}^+}$. At the highest density studied of 10^7 cm^{-3} , the maximum $D_{\text{frac,eq}}^{\text{N}_2\text{H}^+}$ is 0.3. The $D_{\text{frac,eq}}^{\text{N}_2\text{H}^+}$ changes by more than 2 orders of magnitude, from 1.16×10^{-3} at $n_{\text{H}} = 1.00 \times 10^3$ cm^{-3} , to 3.05×10^{-1} at $n_{\text{H}} = 1.00 \times 10^7$ cm^{-3} . From panel (m) we see that, $t_{\text{eq},90}(D_{\text{frac}}^{\text{N}_2\text{H}^+})$ is relatively flat with $n_{\text{H}} \gtrsim 5 \times 10^5$ cm^{-3} . Cores with a range of densities have similar deuteration timescales if other conditions are fixed. When n_{H} is above 6×10^4 cm^{-3} , $t_{\text{eq},90}(D_{\text{frac}}^{\text{N}_2\text{H}^+})$ and $t_{\text{eq},90}(\text{OPR}^{\text{H}_2})$ are more than $10 t_{\text{ff}}$. Thus cores with such densities (and satisfying other fiducial parameters and assuming formation from the adopted initial conditions) that have $D_{\text{frac}}^{\text{N}_2\text{H}^+} \gtrsim 0.1$ would need to be “dynamically old”, i.e. much older than their t_{ff} .

3.4.2 Dependence on T

As shown in panel (j) of Fig. 6, between 5 and 15 K, the $D_{\text{frac,eq}}^{\text{N}_2\text{H}^+}$ profile is quite flat. Above 15 K, $D_{\text{frac,eq}}^{\text{N}_2\text{H}^+}$ drops down by almost 2 orders of magnitude as T approaches 30 K. The maximum $D_{\text{frac,eq}}^{\text{N}_2\text{H}^+}$ of 0.15 is achieved at $T = 13$ K. The profile of $t_{\text{eq},90}(D_{\text{frac}}^{\text{N}_2\text{H}^+})$ is also quite flat across the explored temperatures (panel (n)). We find $t_{\text{eq},90}(D_{\text{frac}}^{\text{N}_2\text{H}^+})$ is always greater than $10 t_{\text{ff}}$ except for the highest temperatures (as is $t_{\text{eq},90}(\text{OPR}^{\text{H}_2})$). At $T \lesssim 15$ K, $\text{OPR}_{\text{eq}}^{\text{H}_2}$ is well below 0.001, but it goes up quickly at higher temperatures. Regions warmer

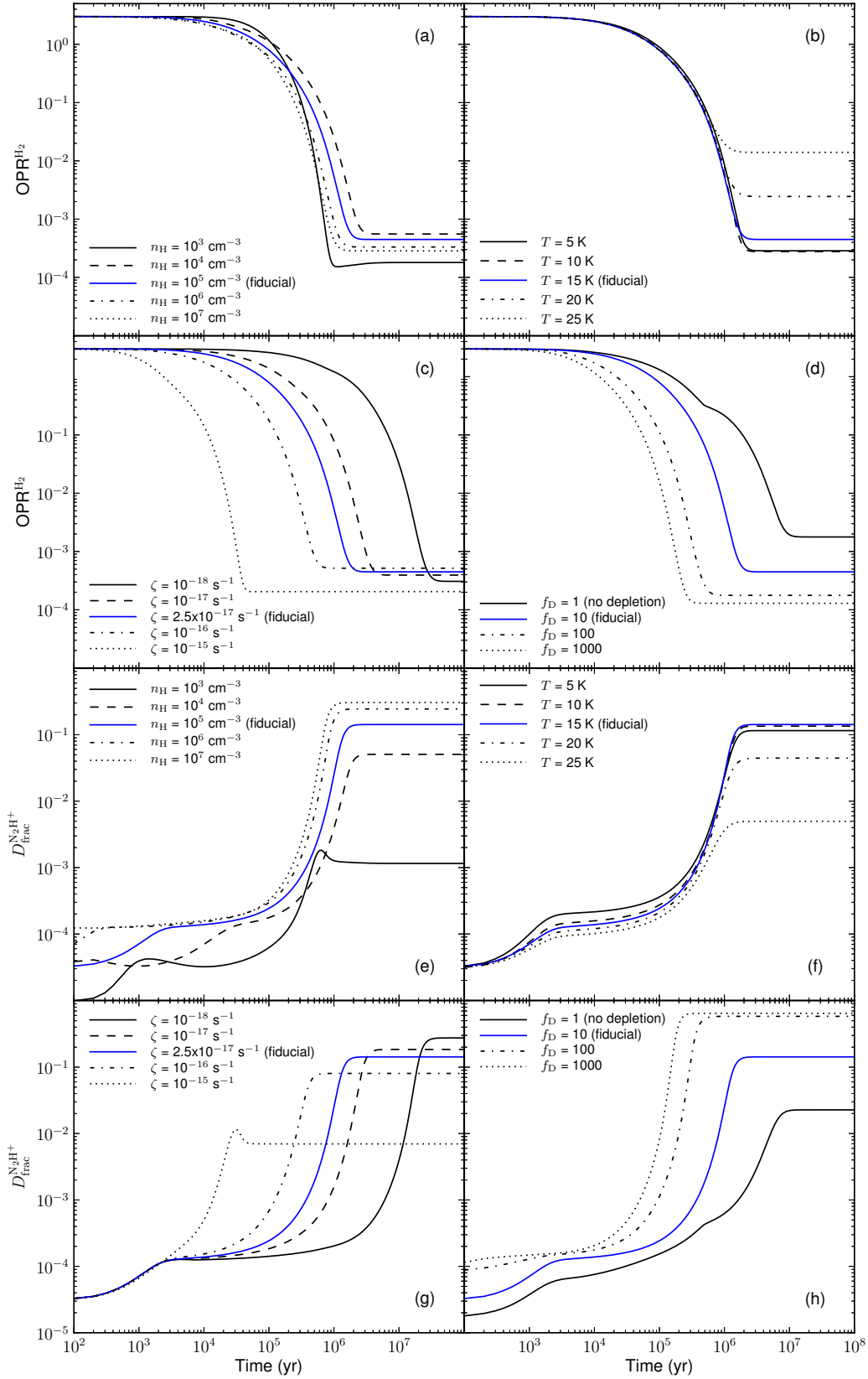


Figure 5. Evolution of OPR^{H_2} and $D_{\text{frac}}^{\text{N}_2\text{H}^+}$ for various densities, temperatures, cosmic ray ionisation rates and depletion factors. The blue solid lines correspond to the fiducial model (Fig. 2). In each case, other parameter values are set to those of the fiducial model. See §3.4 for the complete description of the exploration.

Table 4. Equilibrium values for different initial o/p H₂ ratios.

Starting OPR ^{H₂}	OPR _{eq} ^{H₂} ×10 ⁻⁴	t _{eq} (OPR ^{H₂}) (10 ⁶ yr)	t _{eq,90} (OPR ^{H₂}) (10 ⁶ yr)	D _{frac,eq} ^{N₂H⁺}	t _{eq} (D _{frac} ^{N₂H⁺}) (10 ⁶ yr)	t _{eq,90} (D _{frac} ^{N₂H⁺}) (10 ⁶ yr)
3	4.48	3.14	2.03	0.142	2.78	1.70
1	4.48	3.06	1.95	0.142	2.70	1.62
0.1	4.48	2.72	1.61	0.142	2.34	1.27
0.01	4.48	2.26	1.16	0.142	1.90	0.824
0.001	4.48	1.66	0.557	0.142	1.30	0.351
0.0007	4.48	1.48	0.361	0.142	1.12	0.302

than 20 K, as, for example, gas in the proximity of young stellar objects or regions exposed to enhanced interstellar UV photons, will then experience an increase of the ortho-to-para H₂ ratio and thus a drop in the deuterium fraction (in agreement with findings by Fontani et al. 2011, in high-mass star-forming regions).

3.4.3 Dependence on ζ

$D_{\text{frac,eq}}^{\text{N}_2\text{H}^+}$ drops more than an order of magnitude as ζ increases from 10⁻¹⁸ to 10⁻¹⁵ s⁻¹ (panel (k)), due to the enhanced electron abundance and the consequent dissociative recombination of the deuterated isotopologues of H₃⁺ (see also Caselli et al. 2008). The highest $D_{\text{frac,eq}}^{\text{N}_2\text{H}^+}$ of 0.27 appears at the lowest $\zeta = 10^{-18}$ s⁻¹. This shows the importance for the astrochemical modeling of constraining ζ . Panel (o) shows that $t_{\text{eq},90}(D_{\text{frac}}^{\text{N}_2\text{H}^+})$ changes by almost 3 orders of magnitude within the ζ range explored. The smallest $t_{\text{eq},90}(D_{\text{frac}}^{\text{N}_2\text{H}^+})$ is only 2.33×10⁴ yr at $\zeta = 10^{-15}$ s⁻¹, which is much shorter than t_{ff} . Similar results for the OPR^{H₂} are shown in panel (g) and Fig. A2 (see Appendix A). However, with moderate ζ ($\lesssim 10^{-16}$ s⁻¹), $t_{\text{eq},90}(D_{\text{frac}}^{\text{N}_2\text{H}^+})$ is significantly greater than t_{ff} ($\gtrsim 7 t_{\text{ff}}$).

3.4.4 Dependence on f_D

Panel (l) of Fig. 6 shows that $D_{\text{frac,eq}}^{\text{N}_2\text{H}^+}$ goes up by more than an order of magnitude as f_D increases from 1 to 1000. This agrees with the expectation that depletion of neutral species, in particular CO and O, the main destruction partners of H₃⁺ and its deuterated forms, will result in the enhancement of $D_{\text{frac}}^{\text{N}_2\text{H}^+}$ (see also Dalgarno & Lepp 1984). At $f_D = 300$ we encounter the highest $D_{\text{frac,eq}}^{\text{N}_2\text{H}^+} = 0.73$ in our exploration. Such high values have been measured by Pagani et al. (2009) toward the pre-stellar core L183 and by Fontani et al. (2011) toward cold and quiescent high-mass starless cores. We find $t_{\text{eq},90}(D_{\text{frac}}^{\text{N}_2\text{H}^+})$ decreases with stronger depletion, which is shown in panel (p), although $t_{\text{eq},90}(D_{\text{frac}}^{\text{N}_2\text{H}^+})$ is at least a factor 7 larger than t_{ff} when $f_D \lesssim 100$.

3.5 Comparison to previous results

Compared to previous works, we explore a broader parameter space of physical conditions that is potentially relevant for both high and low-mass cores. In particular, we systematically consider the influence to $D_{\text{frac}}^{\text{N}_2\text{H}^+}$ from a large

range of elemental depletion factors. Pagani et al. (2013) also studied this effect but only for a few depletion values. Parise et al. (2011) studied the effect due to molecular freeze-out in a simpler chemical scheme, not including N₂H⁺. Aikawa et al. (2012) built a comprehensive chemical/dynamical model, including deuterium chemistry, which follows the evolution of pre-stellar cores toward the formation of protostars. However, they do not include spin state chemistry, so comparison with our results cannot be made. Our results show that $D_{\text{frac,eq}}^{\text{N}_2\text{H}^+}$ does not always increase but instead reaches a peak at $f_D = 300$ and drops beyond that. The OPR_{eq}^{H₂} starts to be flat after $f_D = 300$. As discussed in Pagani, Roueff & Lesaffre (2011), the depletion of CO would enrich the deuterated H₃⁺ isotopologues and therefore enrich the deuteration. However, our results show that this effect might be weakened by the consideration of more species and reactions. In addition, at similar level of depletion, our model suggests lower $D_{\text{frac,eq}}^{\text{N}_2\text{H}^+}$. For instance, we ran a model using Pagani et al. (2009) initial conditions and depletion factor, and compared with Figs. 7 and 8 in their paper. In their outer shell, our resulting $D_{\text{frac,eq}}^{\text{N}_2\text{H}^+}$ is smaller than theirs by a factor of ~ 4 . More interestingly, our $t_{\text{eq},90}(D_{\text{frac}}^{\text{N}_2\text{H}^+})$ is longer than theirs by about a factor of 4. Their OPR_{eq}^{H₂} is a factor of about 2.5 lower than our run, and their $t_{\text{eq}}(\text{OPR}^{\text{H}_2})$ is shorter by a similar factor. It is likely that our inclusion of more reactions and species adjusts both equilibrium values and timescales, though a detailed comparison is needed. Parise et al. (2011) benchmarked their results against that of Pagani et al. (2009) and Sipilä et al. (2010), so our difference should be common with these previous works. Wirström et al. (2012) used a network with 4420 reactions, and their equilibrium time for OPR^{H₂} is beyond 10⁶ yr, which is comparable to ours. Sipilä, Caselli & Harju (2013) presented the most comprehensive network, including spin state chemistry, currently available. They included detailed surface chemistry and showed that HD can deplete toward the centre of pre-stellar cores if certain surface reactions including oxygen and molecular hydrogen (with currently unknown rates) can proceed. Our reduced network cannot reproduce their results as surface chemistry is not treated, except for the formation of H₂, HD and D₂ (as explained in Section 2).

There have been a number of discussions regarding the effects of density, temperature, and cosmic-ray ionization rate (e.g. Pagani, Salez, & Wannier 1992; Flower, Pineau Des Forêts & Walmsley 2006; Sipilä et al. 2010; Goldsmith et al. 2011; Pagani et al. 2013). Compared with these previous studies, we focus on $D_{\text{frac,eq}}^{\text{N}_2\text{H}^+}$, our ap-

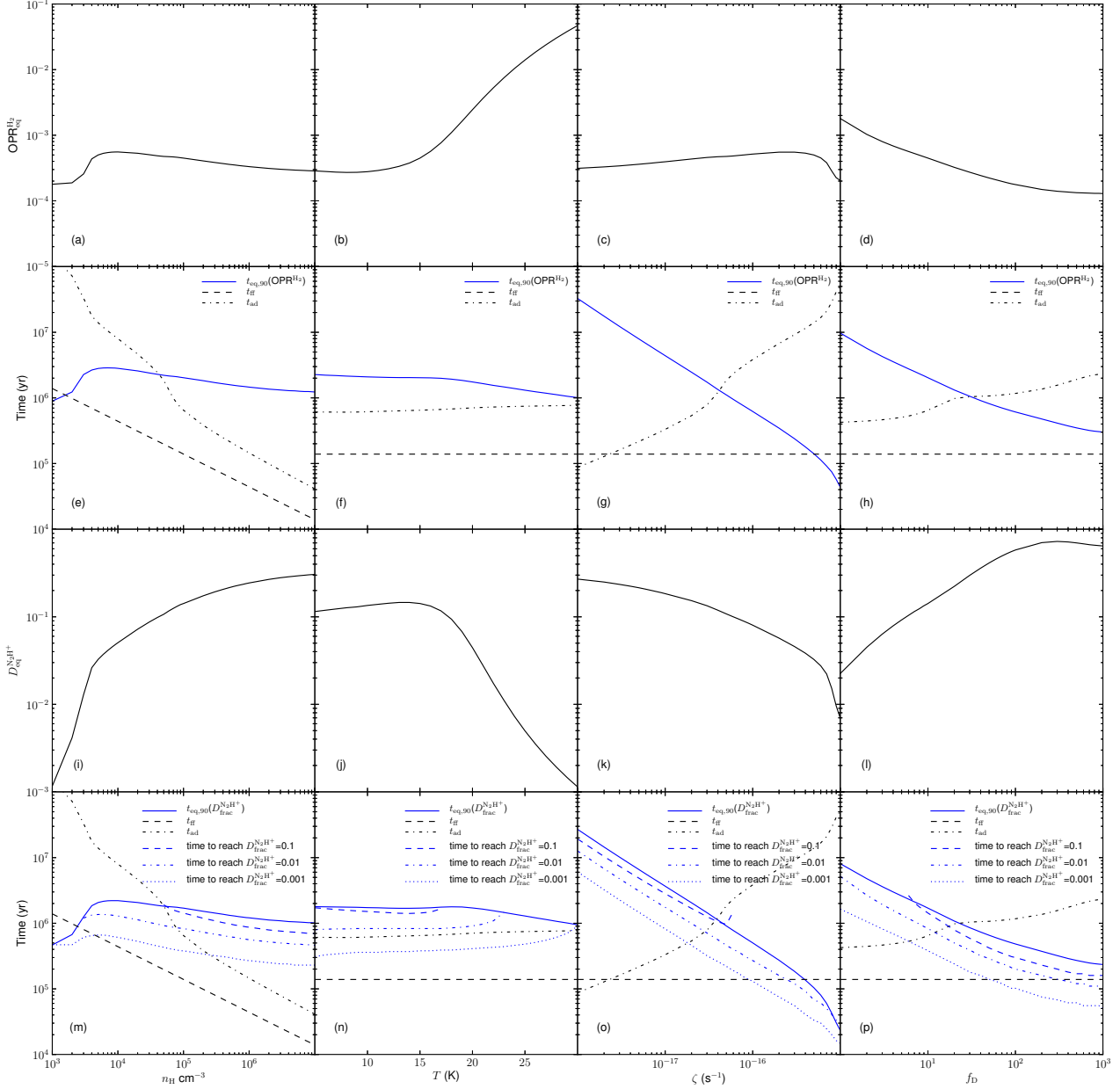


Figure 6. Main results of the parameter-space exploration. From top to bottom rows: $\text{OPR}_{\text{eq}}^{\text{H}_2}$, $t_{\text{eq},90}(\text{OPR}^{\text{H}_2})$, $D_{\text{frac}}^{\text{N}_2\text{H}^+}$, $t_{\text{eq},90}(D_{\text{frac}}^{\text{N}_2\text{H}^+})$ as a function of (left to right) density n_{H} , temperature T , cosmic ray ionisation rate ζ , and depletion factor f_{D} (see §3.2 for definitions). In the 4th row, we also show times to reach $D_{\text{frac}}^{\text{N}_2\text{H}^+} = 0.1, 0.01, 0.001$ (missing portions of the lines imply $D_{\text{frac}}^{\text{N}_2\text{H}^+}$ does not reach the value of interest for these conditions). Also shown are t_{ff} (Eq. 3) and t_{ad} (§4.3) to be compared to $t_{\text{eq},90}(\text{OPR}^{\text{H}_2})$ and $t_{\text{eq},90}(D_{\text{frac}}^{\text{N}_2\text{H}^+})$.

proach is more systematic and it uses more complete cold core chemistry. Compared with the steady-state models in Sipilä et al. (2010) (their Figs. 3 and 4, explorations of density and temperature), our results (Fig. 6a,b) show almost identical profile for $\text{OPR}_{\text{eq}}^{\text{H}_2}$, but encompass broader conditions. The absolute $\text{OPR}_{\text{eq}}^{\text{H}_2}$ values are not the same because we used different initial conditions. Pagani et al. (2013) presented parameter space explorations with coupled dynamical history, e.g. the effects on $D_{\text{frac}}^{\text{N}_2\text{H}^+}$ from ζ . Our results generally agree (also with Goldsmith et al. 2011), while Pagani et al. (2013) also distinguished between fast and slow

collapses. However, as stated earlier, our goal is to first set up a systematic exploration of chemistry independent of assumed prior dynamical history. We will then use these as a basis for future studies of more realistic models that include dynamics.

4 DISCUSSION

From the above sections, it is clear that the deuteration age of a starless core can be gauged only if detailed observa-

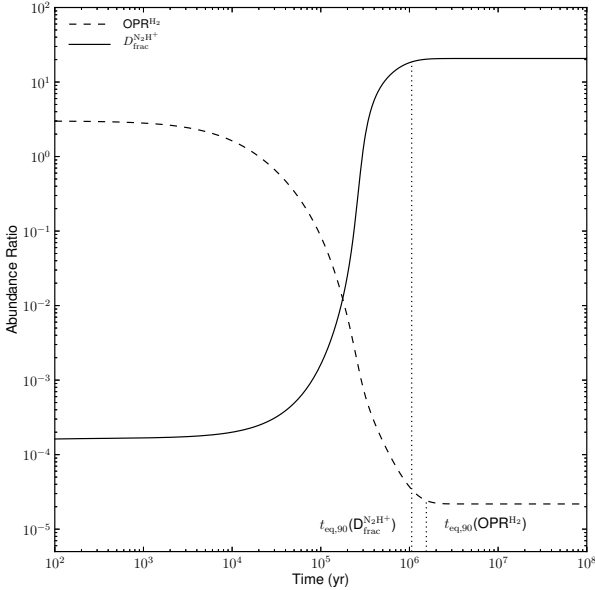


Figure 7. The evolution of OPR^{H_2} and $D_{\text{frac}}^{\text{N}_2\text{H}^+}$ under physical conditions: $n_{\text{H}} = 10^7 \text{ cm}^{-3}$, $T = 13 \text{ K}$, $\zeta = 10^{-18} \text{ s}^{-1}$, $f_D = 300$. This setup gives highest value of $D_{\text{frac,eq}}^{\text{N}_2\text{H}^+}$ of the models explored (not necessarily a formal global maximum). Results are also listed in Table 5.

tions of key molecular ions are available and if the physical structure and environment of the core are well known. This is why it is important to focus this analysis on relatively simple cores, preferably embedded in quiescent molecular clouds, to avoid protostellar feedback effects. Below, we discuss some special cases.

4.1 Highest $D_{\text{frac}}^{\text{N}_2\text{H}^+}$ predicted in our model

High values of $D_{\text{frac}}^{\text{N}_2\text{H}^+}$ have been reported in recent observations. Fontani et al. (2011) observed several potential massive starless cores, finding a highest $D_{\text{frac}}^{\text{N}_2\text{H}^+} = 0.7$ in their source Infrared Dark Cloud G2. An even higher value of $D_{\text{frac}}^{\text{N}_2\text{H}^+} = 0.99$ has been reported by Miettinen et al. (2012, though this may be affected by the uncertainties from treating N_2H^+ with non-LTE model but N_2D^+ with LTE model), toward Orion B9 SMM1. Such high values are not predicted by our fiducial model. However, it is interesting if we combine the explored parameters n_{H} , T , ζ , f_D at the values where $D_{\text{frac,eq}}^{\text{N}_2\text{H}^+}$ peaks ($n_{\text{H}} = 10^7 \text{ cm}^{-3}$, $T = 13 \text{ K}$, $\zeta = 10^{-18} \text{ s}^{-1}$, $f_D = 300$) to gauge the global maximum level of deuteration that can result from our model. A model with these conditions is shown in Fig. 7. Equilibrium ratios and timescales are summarized in Table 5. We find $D_{\text{frac}}^{\text{N}_2\text{H}^+}$ goes up to 20.7, while $t_{\text{eq},90}(D_{\text{frac}}^{\text{N}_2\text{H}^+})$ is about $76 t_{\text{ff}}$ ($1.39 \times 10^4 \text{ yr}$ at $n_{\text{H}} = 10^7 \text{ cm}^{-3}$). Thus, extreme deuteration is indeed possible and the large values measured can be obtained with reasonable values of the model parameters.

4.2 From observed $D_{\text{frac}}^{\text{N}_2\text{H}^+}$ to core age

To derive the core age, ideally we would run a model with accurately-determined physical conditions, including the environmental variable ζ , and read out the time to reach the observed $D_{\text{frac}}^{\text{N}_2\text{H}^+}$. However, there are typically large uncertainties in measuring the physical structure. Note also that if the core is close to chemical equilibrium, then the derived deuteration timescale is only a lower limit to its age.

In one of the best studied low-mass pre-stellar cores, L1544 in the Taurus molecular cloud, we can attempt to define an age. Within the central 3600 AU (the beam size of the IRAM 30 m antenna at the frequency of the $\text{N}_2\text{H}^+(1-0)$ line), $D_{\text{frac}}^{\text{N}_2\text{H}^+} = 0.2^3$ (Crapsi et al. 2005), the average number density is $n_{\text{H}} \simeq 10^6 \text{ cm}^{-3}$ (Keto & Caselli 2010), the temperature is about 6 K (Crapsi et al. 2007), the cosmic ray ionisation rate is $\simeq 1 \times 10^{-17} \text{ s}^{-1}$ and the CO depletion factor is 100 (Keto & Caselli 2010). With these parameters, we obtain deuteration timescales of $3.3 \times 10^5 \text{ yr} - 2.1 \times 10^5 \text{ yr}$, starting with $\text{OPR}^{\text{H}_2} = 3-0.1$, respectively, i.e. between 7.5 and $4.8 t_{\text{ff}}$. At the time of best agreement with the $D_{\text{frac}}^{\text{N}_2\text{H}^+}$ measurements, the OPR^{H_2} is 3.2×10^{-3} .

In cases where such a detailed analysis cannot be carried out, we can still derive some limits on the core deuteration timescale. For example, $D_{\text{frac}}^{\text{N}_2\text{H}^+} \gtrsim 0.1$ has been measured in low-mass pre-stellar cores (Crapsi et al. 2005; Pagani et al. 2009) and high-mass starless cores (Fontani et al. 2011; Miettinen et al. 2012), and there are currently no values of $D_{\text{frac}}^{\text{N}_2\text{H}^+}$ observed to be greater than 1. Starting from this, we examine all models in our parameter space exploration (§3.4) to find how long it takes for $D_{\text{frac}}^{\text{N}_2\text{H}^+}$ to reach 0.1. The results are shown as the blue dashed lines in the 4th row of Fig. 6. The “missing” parts indicate conditions under which $D_{\text{frac}}^{\text{N}_2\text{H}^+}$ fails to reach 0.1. As one can see from the figure, to reach $D_{\text{frac}}^{\text{N}_2\text{H}^+} > 0.1$, the cores should be dense ($n_{\text{H}} \gtrsim 5 \times 10^4 \text{ cm}^{-3}$), cold ($T \lesssim 17 \text{ K}$), at least moderately depleted ($f_D \gtrsim 6$), and with moderate cosmic-ray fluxes ($\zeta \lesssim 6 \times 10^{-17} \text{ s}^{-1}$). In all cases, the time to reach $D_{\text{frac}}^{\text{N}_2\text{H}^+} = 0.1$ are longer than t_{ff} . With moderate depletion ($f_D \lesssim 100$), the large $D_{\text{frac}}^{\text{N}_2\text{H}^+}$ ($\gtrsim 0.1$) is likely to indicate a large deuteration age (\gtrsim several t_{ff}) for the observed starless cores.

One way to have shorter deuteration timescales of the cores is if the starting OPR^{H_2} values, inherited from the parent cloud, are small (see Appendix A and discussions in Pagani, Roueff & Lesaffre 2011). While this possibility cannot be completely ruled out, it would appear to itself require relatively long-lived parental clouds. More stringent constraints may result from comparing the relative variation of $D_{\text{frac}}^{\text{N}_2\text{H}^+}$ across a given cloud, i.e. its relative enhancement in a core compared to the surrounding natal clump. Improvement in the theoretical modeling, planned for a future study, will involve time-dependent evolution of the density and depletion and eventual coupling of the deuteration

³ We note that this observed $D_{\text{frac}}^{\text{N}_2\text{H}^+}$ value should be treated as a lower limit, as this is an average along the line of sight and it is well known that the $\text{N}_2\text{H}^+(1-0)$ emission is more extended than the $\text{N}_2\text{D}^+(2-1)$ emission (Caselli et al. 2002). Therefore, our estimates of the time scales are also lower limits.

Table 5. Equilibrium values for the maximum deuterium fraction obtained in our modeling

$\text{OPR}_{\text{eq}}^{\text{H}_2}$ ($\times 10^{-4}$)	$t_{\text{eq}}(\text{OPR}^{\text{H}_2})$ (10^6 yr)	$t_{\text{eq},90}(\text{OPR}^{\text{H}_2})$ (10^6 yr)	$D_{\text{frac,eq}}^{\text{N}_2\text{H}^+}$	$t_{\text{eq}}(D_{\text{frac}}^{\text{N}_2\text{H}^+})$ (10^6 yr)	$t_{\text{eq},90}(D_{\text{frac}}^{\text{N}_2\text{H}^+})$ (10^6 yr)
0.218	2.90	1.55	20.7	2.38	1.06

chemical network to (magneto-)hydrodynamic simulations of cloud evolution.

4.3 Ambipolar diffusion time

The ambipolar diffusion timescale t_{ad} (the timescale for neutrals in dense cores with low ionisation fractions to contract relative to the magnetic field) can be calculated using the expression $t_{\text{ad}} = 2.5 \times 10^{13} x(e)$ yr (Spitzer 1978; Shu, Adams & Lizano 1987) (also see Bodenheimer 2011, but with a slightly different assumption), where $x(e)$ is the electron abundance relative to n_{H} . Fig. 6 plots t_{ad} , to compare with $t_{\text{eq},90}(D_{\text{frac}}^{\text{N}_2\text{H}^+})$ and t_{ff} . As t_{ad} is closely related to the ionisation structure in core, high density and low ζ reduce t_{ad} , as shown in panels (e), (g), (m) and (o). There is no universal relation between t_{ad} and the deuteration timescale in our exploration, but there is the well-known trend that t_{ad} is longer than t_{ff} .

For the observed cores discussed in §4.2, where the time to reach the observed deuteration level may indicate relatively old cores compared to their t_{ff} , then this would likely require that magnetic fields were playing a role in regulating core contraction. Then we may expect core ages to be similar to t_{ad} , which, in this context, provides an additional constraint to combined physical and chemical modeling of these systems.

5 CONCLUSIONS

This paper has presented a parameter space exploration of the deuterium fractionation process, in particular of N_2H^+ , in conditions appropriate to starless dense cloud cores in different environments. Deuterium and spin state chemistry has been included in a reduced chemical network extracted from the KIDA database. The main results of the paper are as follows:

- The deuterium fraction of N_2H^+ increases with increasing density, decreasing temperature, decreasing cosmic-ray ionisation rate and increasing freeze-out. The maximum deuterium fraction reached by our model is about 20 (never observed so far) and can be reached if the volume density is 10^7 cm^{-3} , the temperature is 13 K, the cosmic-ray ionisation rate is 10^{-18} s^{-1} and the depletion factor is 300.
- When the gas temperature exceeds $\simeq 20$ K, the ortho-to-para H_2 ratio increases, reducing the deuterium fraction, so that warmer starless cores should display lower deuterium fractions (as recently found in high-mass star-forming regions).
- The above findings are robust against changes in the initial elemental and molecular abundances in the chemical model.
- Constraints on core ages can be obtained if accurate measurements of the deuterium fraction are made and the physical structure and cosmic ray ionisation rate are known. In

the case of the well-known low-mass pre-stellar core L1544, the gas within the central 3600 AU has a deuteration age between $\simeq 5$ and 8 times the free-fall time, depending on the initial value of the ortho-to-para H_2 ratio.

- More generally, to reproduce the typical deuterium fractions measured toward low-mass and massive pre-stellar cores ($\gtrsim 0.1$), the following physical parameters are needed: $n_{\text{H}} \gtrsim 5 \times 10^4 \text{ cm}^{-3}$, $T \lesssim 17$ K, depletion factor $\gtrsim 6$, and cosmic ray ionisation rate $\lesssim 6 \times 10^{-17} \text{ s}^{-1}$. In general, these values of deuterium fractions require timescales several times longer than the free-fall timescale. This suggests that dense cores with large deuterium fractions are dynamically old, likely requiring support against gravity by magnetic fields. These conclusions can be avoided if the cosmic ray ionisation rate is very high ($\gtrsim 10^{-16} \text{ s}^{-1}$) or if the initial ortho-to-para ratio of H_2 in the core is very small ($\lesssim 0.01$), although this last condition itself requires the parental cloud to have a significant age.

ACKNOWLEDGMENTS

The authors acknowledge the continuous and fruitful interactions with Olli Sipilä and Jorma Harju. SK acknowledges support from Xueying Tang and an NRAO Student Observing Support grant. JCT acknowledges support from Univ. of Florida Research Opportunity Seed Fund and the Florida Space Inst. VW acknowledges funding by the French INSU/CNRS program PCMI, the Observatoire Aquitain des Sciences de l'Univers and the European Research Council (ERC Grant 336474: 3DICE).

REFERENCES

- Aikawa Y., Wakelam V., Hersant F., Garrod R.T., Herbst E., 2012, *ApJ*, 760, 40
- Bacmann A., Lefloch B., Ceccarelli C., Steinacker J., Castets A., Loinard L., 2003, *ApJ*, 585, L55
- Bergin E.A., Plume R., Williams J.P., Myers P.C., 1999, *ApJ*, 512, 724
- Bisschop S.E., Fraser H.J., Öberg K.I., van Dishoeck E.F., Schlemmer S., 2006, *A&A*, 449, 1297
- Bodenheimer P.H., 2011, *Principles of Star Formation*. Springer, Berlin
- Butler M., Tan J., 2012, *ApJ*, 754, 5
- Caselli P., 2002, *P&SS*, 50, 1133
- Caselli P., Walmsley C.M., Terziewa R., Herbst E., 1998, *ApJ*, 499, 234
- Caselli P., Walmsley C.M., Tafalla M., Dore L., Myers P.C., 1999, *ApJ*, 523, L165
- Caselli P., Walmsley C.M., Zucconi A., Tafalla M., Dore L., Myers P.C., 2002, *ApJ*, 565, 344

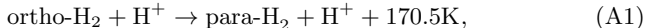
- Caselli P., Vastel C., Ceccarelli C., van der Tak F.F.S., Crapsi A., Bacmann A., 2008, *A&A*, 492, 703
- Ceccarelli C., Hily-Blant P., Montmerle T., Dubus G., Galant Y., Fiasson A., 2011, *ApJ*, 740, L4
- Crabtree K.N., Indriolo N., Kreckel H., Tom B.A., McCall B.J., 2011, *ApJ*, 729, 15
- Crapsi A., Caselli P., Walmsley C.M., Myers P.C., Tafalla M., Lee C.W., Bourke T.L., 2005, *ApJ*, 619, 379
- Crapsi A., Caselli P., Walmsley M.C., Tafalla M., 2007, *A&A*, 470, 221
- Dalgarno A., 2006, *PNAS*, 103, 12269
- Dalgarno A., Lepp S., 1984, *ApJ*, 287, L47
- Draine B.T., Sutin B., 1987, *ApJ*, 320, 803
- Emprechtinger M., Caselli P., Volgenau N.H., Stutzki J., Wiedner M.C., 2009, *A&A*, 493, 89
- Flower D.R., Pineau Des Forêts G., Walmsley C.M., 2006, *A&A*, 449, 621
- Fontani F., Caselli P., Crapsi A., Cesaroni R., Molinari S., Testi L., Brand J., 2006, *A&A*, 460, 709
- Fontani F., Zhang Q., Caselli P., Bourke T.L., 2009, *A&A*, 499, 233
- Fontani F. et al., 2011, *A&A*, 529, L7
- Friesen R.K., Di Francesco J., Myers P.C., Belloche A., Shirley Y.L., Bourke T.L., André P., 2010, *ApJ*, 718, 666
- Goldsmith P.F., et al., 2011, *ApJ*, 737, 96
- Guelin M., Langer W.D., Snell R.L., Wootten H.A., 1977, *ApJ*, 217, 165
- Hernandez A.K., Tan J.C., Caselli P., Butler M.J., Jimnez-Serra I., Fontani F., Barnes P., 2011, *ApJ*, 738, 11
- Hily-Blant P., Walmsley M., Pineau des Forêts G., Flower D., 2010, *A&A*, 513, A41
- Hugo E., Asvany O., Schlemmer S., 2009, *J. Chem. Phys.*, 130, 164302
- Indriolo N., McCall B.J., 2012, *ApJ*, 745, 91
- Keto E., Caselli P., 2010, *MNRAS*, 402, 1625
- Li X., Heays A.N., Visser R., Ubachs W., Lewis B.R., Gibson S.T., van Dishoeck E.F., 2013, *A&A*, 555, 14
- Miettinen O., Harju J., Haikala L.K., Juvela M., 2012, *A&A*, 538, 137
- Oliveira C.M., Hébrard G., Howk J.C., Wruk J.W., Chayer P., Moos H.W., 2003, *ApJ*, 587, 235
- Padovani M., Galli D., Glassgold A.E., 2009, *A&A*, 501, 619
- Pagani L., Salez M., Wannier P.G., 1992, *A&A*, 258, 479
- Pagani L. et al., 2009, *A&A*, 494, 623
- Pagani L., Roueff E., Lesaffre P., 2011, *ApJ*, 739, L35
- Pagani L., Lesaffre P., Jorfi M., Honvault P., González-Lezana T., Faure A., 2013, *A&A*, 551, 38
- Parise B., Belloche A., Du F., Güsten R., Menten K.M., 2011, *A&A*, 526, 31
- Pillai T., Wyrowski F., Carey S.J., Menten K.M., 2006, *A&A*, 450, 569
- Pillai T., Wyrowski F., Hatchell J., Gibb A.G., Thompson M.A., 2007, *A&A*, 467, 207
- Pillai T., Caselli P., Kauffmann J., Zhang Q., Thompson M.A., Lis D.C., 2012, *ApJ*, 751, 135
- Pineau des Forêts G., Flower D.R., McCarroll R., 1991, *MNRAS*, 248, 173
- Ragan S.E., Bergin E.A., Wilner D., 2011, *ApJ*, 736, 163
- Shu F.H., Adams F.C., Lizano S., 1987, *ARA&A*, 25, 23
- Sipilä O., Hugo E., Harju J., Asvany O., Juvela M., Schlemmer S., 2010, *A&A*, 509, 98
- Sipilä O., Caselli P., Harju J., 2013, *A&A*, 554, 92
- Spitzer L., Jr, 1978, *Physical Processes in the Interstellar Medium*. Princeton Univ. Press, Princeton, NJ
- Troscompt N., Faure A., Maret S., Ceccarelli C., Hily-Blant P., Wiesenfeld L., 2009, *A&A*, 506, 1243
- van der Tak F.F.S., van Dishoeck E.F., 2000, *A&A*, 358, L79
- Vastel C. et al., 2012, *A&A*, 547, 33
- Wakelam V., Herbst E., 2008, *ApJ*, 680, 371
- Wakelam V. et al., 2012, *ApJS*, 199, 21
- Walmsley C.M., Flower D.R., Pineau des Forêts G., 2004, *A&A*, 418, 1035
- Ward-Thompson D., Motte F., Andre P., 1999, *MNRAS*, 305, 143
- Wirström E.S., Charnley S.B., Cordiner M.A., Milam S.N., 2012, *ApJ*, 757, L11
- Wootten A., Snell R., Glassgold A.E., 1979, *ApJ*, 234, 876

APPENDIX A: THE INITIAL OPR^{H2} IN THE CORE AND THE AGE OF THE PARENTAL CLOUD

With a low initial value of OPR^{H2} in the core, even if the equilibrium deuteration level is high, the deuteration timescale can be short. Since some chemical evolution progresses in the precursor low-density molecular cloud, the initial OPR^{H2} in the core is approximately the final OPR^{H2} in the cloud. We need to know how long the parental cloud has evolved and constrain the initial OPR^{H2} for the core. We also need to be aware of how physical properties influence OPR^{H2} and $D_{\text{frac}}^{\text{N}_2\text{H}^+}$. In the following, we consider the evolution of OPR^{H2} in lower density clouds and measure how long it takes for OPR^{H2} to reach the initial values explored in §3.3.2.

For the parental cloud, the reference initial physical conditions are set to $n_{\text{H}} = 1.0 \times 10^4 \text{ cm}^{-3}$, $T = 15 \text{ K}$, $\zeta = 2.5 \times 10^{-17}$, $f_{\text{D}} = 1$ (no depletion), and $A_{\text{V}} = 10$. The equilibrium ratios and timescales are summarized in Table A1. We then consider a range of n_{H} , T , and ζ , to see how OPR^{H2} and $D_{\text{frac}}^{\text{N}_2\text{H}^+}$ behave in a variety of parental clouds (e.g. Giant Molecular Clouds, GMCs). This is illustrated in Fig. A1 for some representative physical properties. The main point here is that ζ impacts both the final values of the ratios and the timescales for equilibration, while n_{H} and T mainly affect the equilibrium ratios.

In Fig. A2, we plot the time to reach OPR^{H2} values of 0.1, 0.01, and 0.001. An enhancement of ζ reduces the time to reach these values OPR^{H2}, while the variation of density and temperature have little effect. Strong ionisation from a high value of ζ increases the H⁺ abundance, so a faster H₂ ortho-para conversion proceeds via the exothermic reaction



and a shorter timescale to reach equilibrium results. This in turn influences $D_{\text{frac}}^{\text{N}_2\text{H}^+}$. Since cosmic-rays are the major ionising source in dense cores, ζ has large effect on our estimation of the initial OPR^{H2} for the core. Although large values of ζ (10^{-15} – 10^{-16} s^{-1}) may be expected in diffuse clouds (e.g. Indriolo & McCall 2012) or nearby strong cosmic ray sources, such as supernovae remnants (e.g. Ceccarelli et al. 2011), lower values (of the order of $1\text{--}3 \times 10^{-17} \text{ s}^{-1}$) have been estimated in molecular clouds in our Galaxy (van der Tak & van Dishoeck 2000; Keto & Caselli 2010), suggesting a drop in the cosmic ray flux from diffuse to dense clouds (see also discussion in Padovani, Galli & Glassgold 2009). For $\zeta = 2.5 \times 10^{-17} \text{ s}^{-1}$ as adopted in our fiducial model, and within the explored ranges of density and temperature, it takes either close to or above 1 million years for OPR^{H2} to drop to 0.1 (minimum 0.85 Myr in our exploration). If the parental cloud is older than this timescale, then the initial OPR^{H2} may drop to values that begin to significantly affect (shorten) the deuteration timescale of N₂H⁺.

Thus any constraints on core deuteration timescales also involve assumptions about the prior history of the initial cloud. Observational estimates of OPR^{H2} in clouds and dense cores are uncertain (Pagani et al. 2009; Troscompt et al. 2009), and more observations are needed to put stringent constraints on this important parameter.

As a further investigation, we carry out three more ex-

plorations, similar to those of §3.4, but with initial OPR^{H2} = 1, 0.1, 0.01. The results are summarized in Figs. A3, A4, and A5. The major point here is that with these low initial OPR^{H2}, the $t_{\text{eq},90}(D_{\text{frac}}^{\text{N}_2\text{H}^+})$ is still several times longer than the free-fall timescale, given the typical conditions.

This paper has been typeset from a T_EX/L^AT_EX file prepared by the author.

Table A1. Equilibrium values for the parental cloud model

$\text{OPR}_{\text{eq}}^{\text{H}_2}$ ($\times 10^{-4}$)	$t_{\text{eq}}(\text{OPR}^{\text{H}_2})$ (10^6 yr)	$t_{\text{eq},90}(\text{OPR}^{\text{H}_2})$ (10^6 yr)	$D_{\text{frac,eq}}^{\text{N}_2\text{H}^+}$	$t_{\text{eq}}(D_{\text{frac}}^{\text{N}_2\text{H}^+})$ (10^6 yr)	$t_{\text{eq},90}(D_{\text{frac}}^{\text{N}_2\text{H}^+})$ (10^6 yr)
22.1	14.6	4.21	0.0172	12.4	9.17

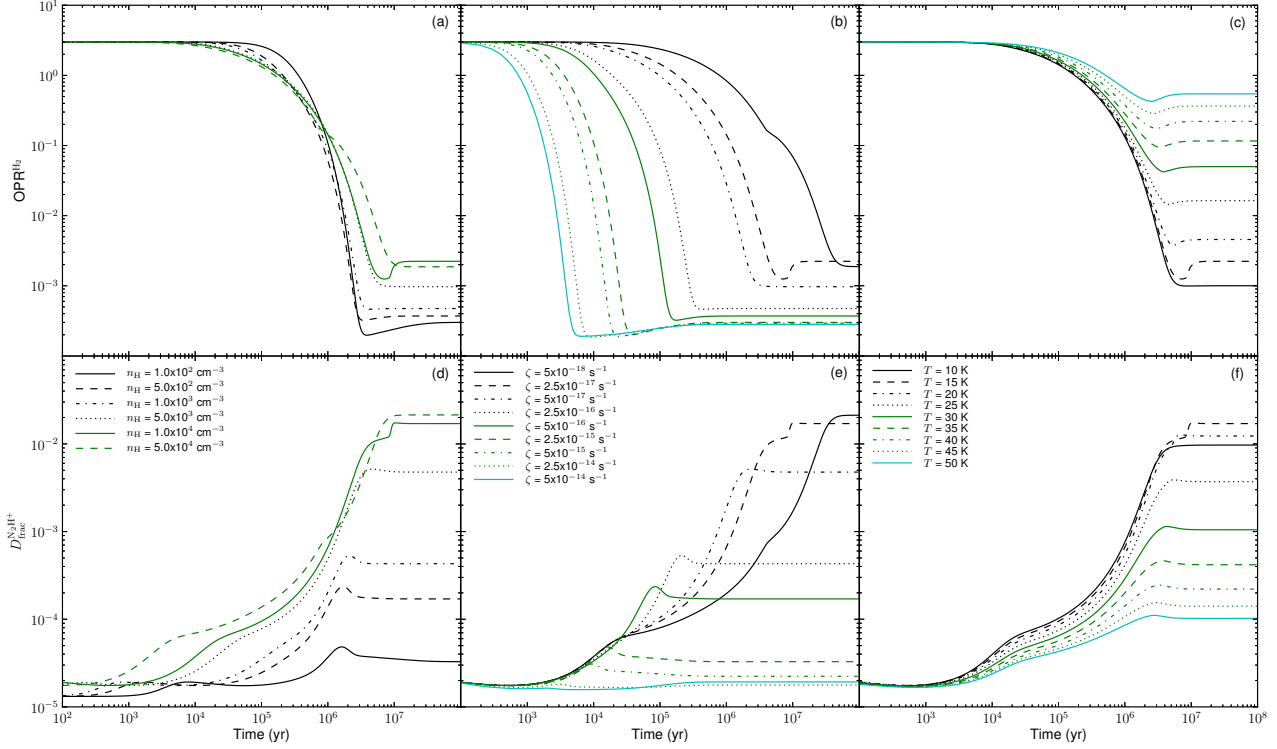


Figure A1. Evolution of OPR^{H_2} and $D_{\text{frac}}^{\text{N}_2\text{H}^+}$ in a parental molecular cloud with no depletion. Each set of legends corresponds to the two figures in that particular column. Panels (a) and (d) show different chemical evolution paths with different n_{H} , fixing $\zeta = 2.5 \times 10^{-17} \text{ s}^{-1}$, $T = 15 \text{ K}$; panels (b) and (e) show the variation with ζ , fixing $n_{\text{H}} = 10^4 \text{ cm}^{-3}$, $T = 15 \text{ K}$; panels (c) and (f) show the variation with T , fixing $n_{\text{H}} = 10^4 \text{ cm}^{-3}$, $\zeta = 2.5 \times 10^{-17} \text{ s}^{-1}$.

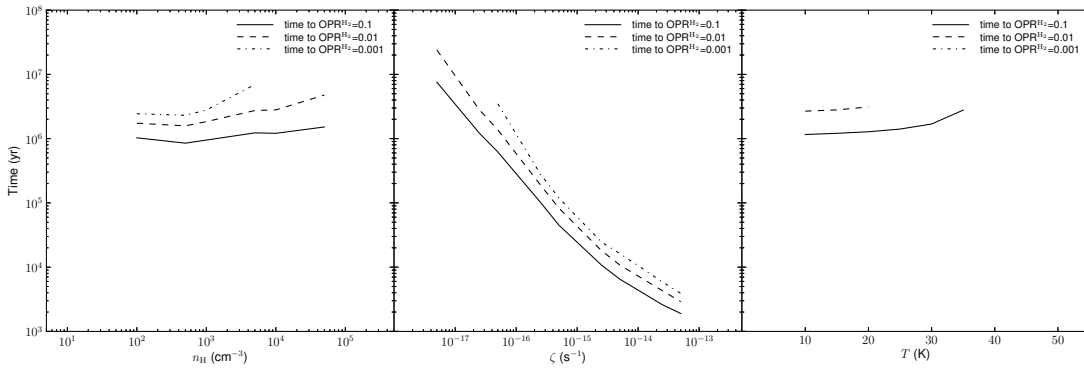


Figure A2. Time to reach $\text{OPR}^{\text{H}_2} = 0.1, 0.01, 0.001$ in the parental cloud. Regions where the lines are missing indicate that the system never reaches the relevant OPR^{H_2} .

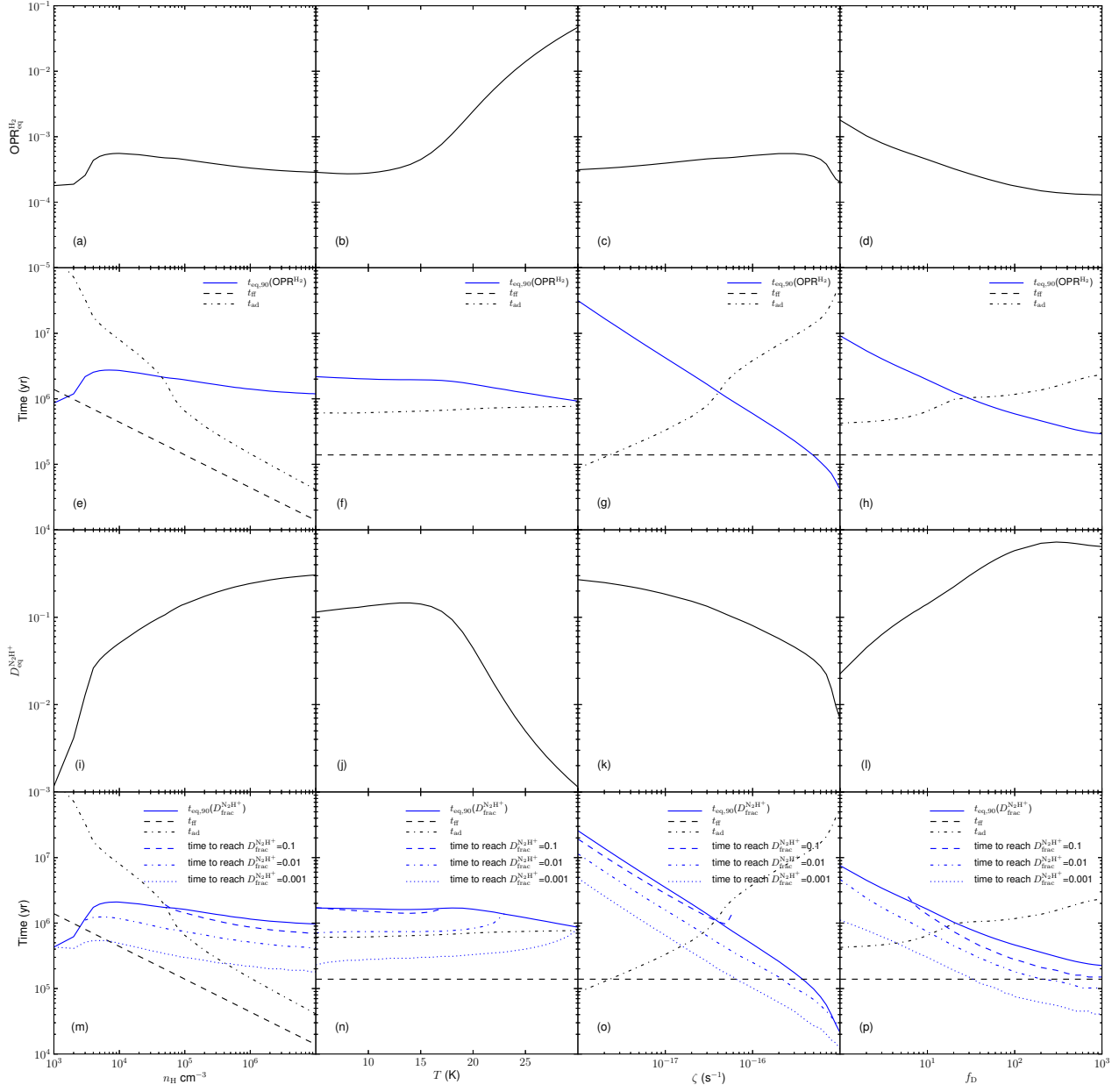


Figure A3. Same as Fig. 6, except for initial $OPR^{H_2} = 1$.

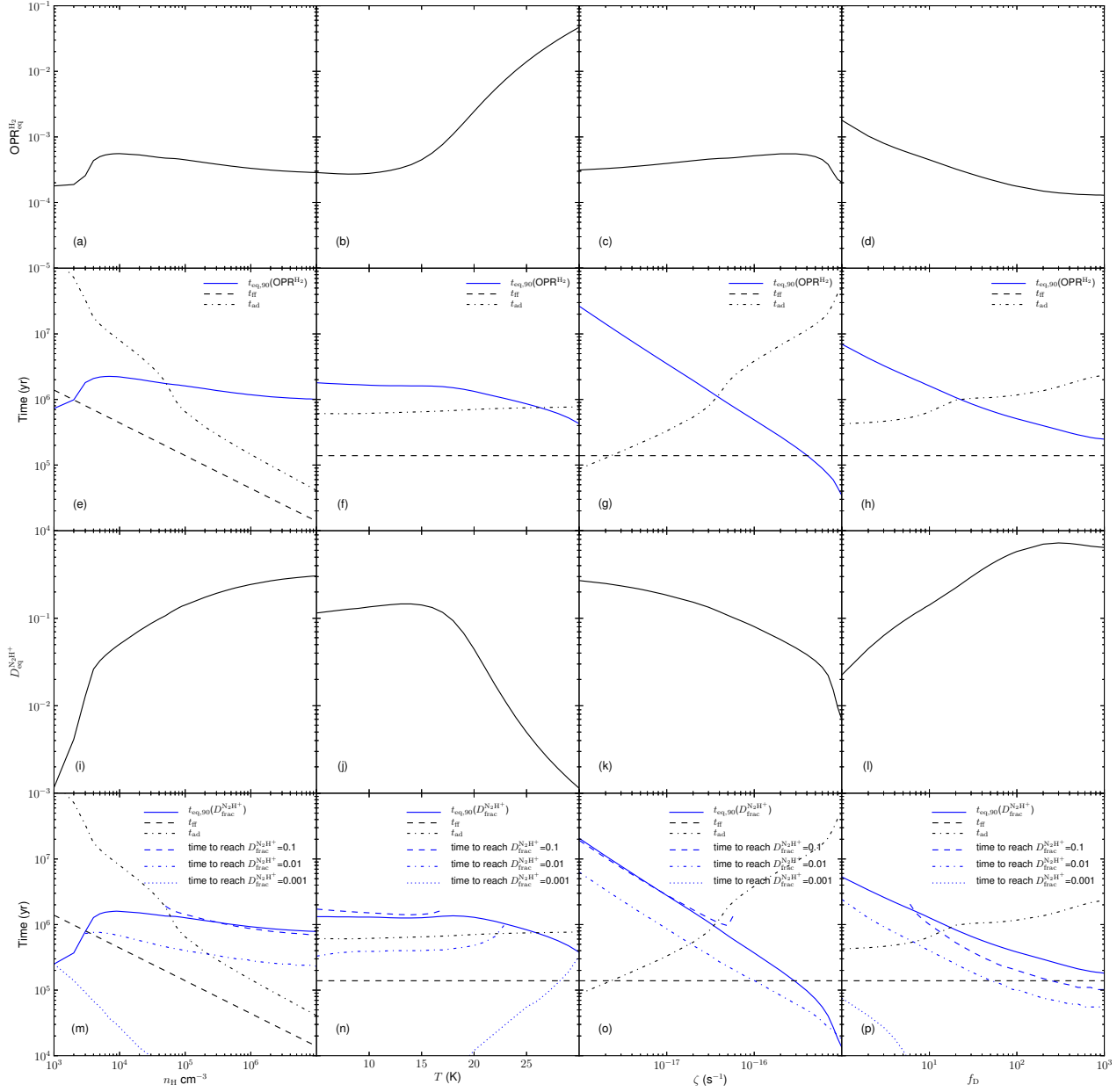


Figure A4. Same as Fig. 6, except for initial $OPR^{H_2} = 0.1$.

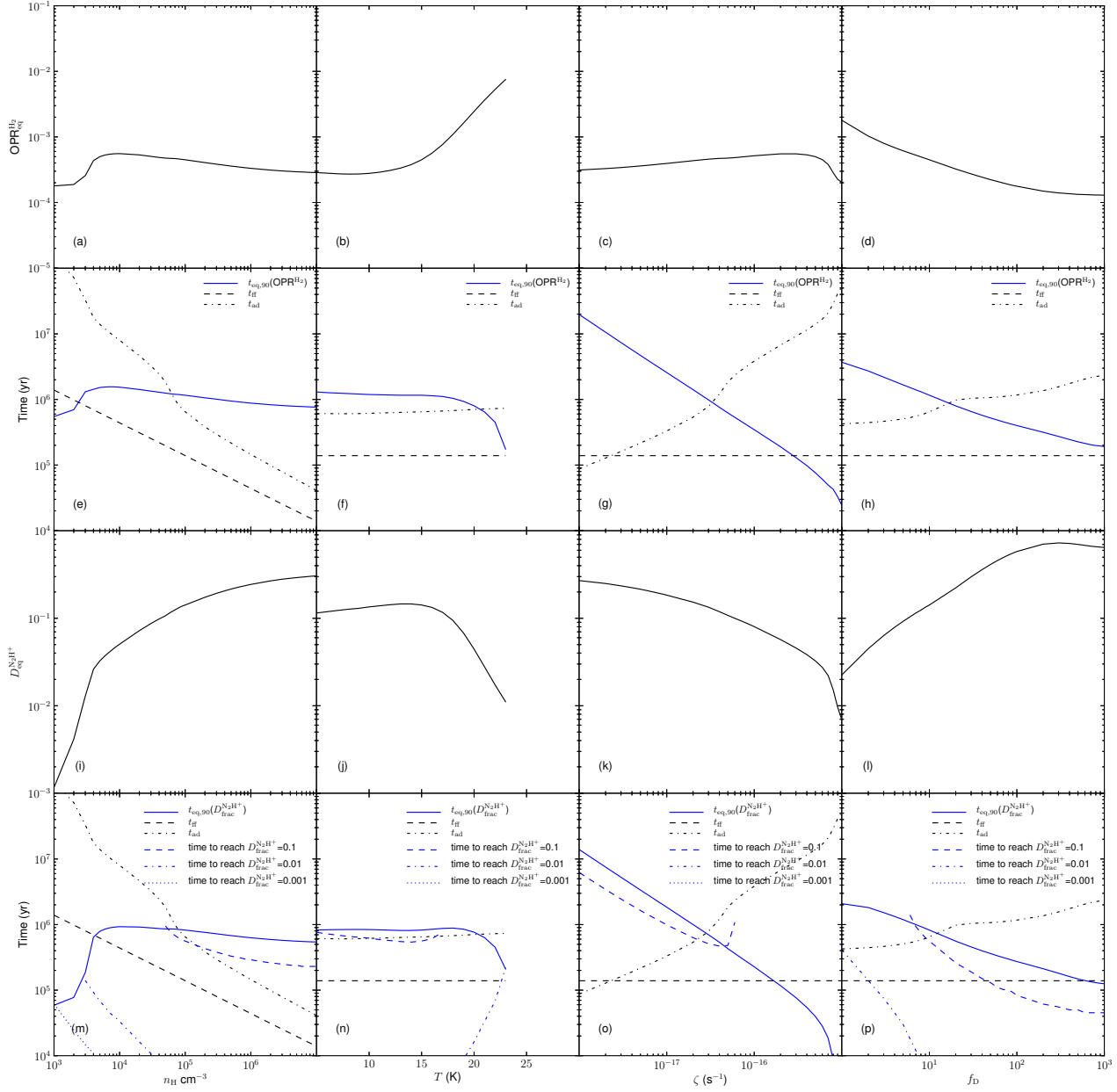


Figure A5. Same as Fig. 6, except for initial $\text{OPR}^{\text{H}_2} = 0.01$. The blank parts in high-temperature exploration are due to that initial OPR^{H_2} is smaller than $\text{OPR}_{\text{eq}}^{\text{H}_2}$, see panel (b) in Fig. 6.